



# Synthesis of monodisperse highly nitrogen-rich porous carbon microspheres for CO<sub>2</sub> adsorption

Shou-De Han<sup>1,2</sup> · Qun-Yan Li<sup>1,2</sup> · Jun-Guo Liu<sup>3</sup> · Ya-Li Wang<sup>1,2</sup> · Qi Wei<sup>1,2</sup> · Su-Ping Cui<sup>1,2</sup>

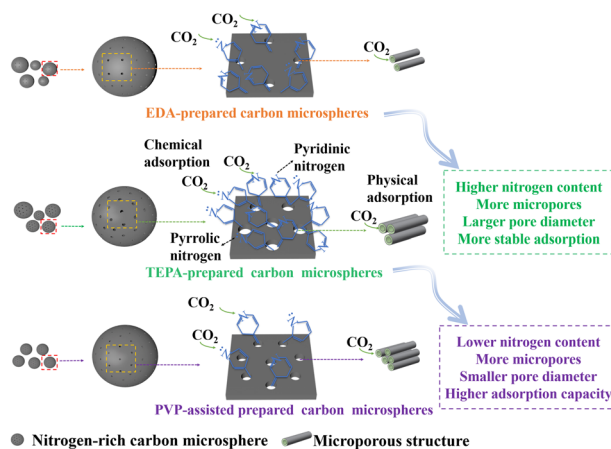
Received: 18 January 2023 / Accepted: 5 June 2023 / Published online: 10 July 2023

© The Author(s), under exclusive licence to Springer Science+Business Media, LLC, part of Springer Nature 2023

## Abstract

The nitrogen-rich carbon microspheres were prepared by the one-pot hydrothermal synthesis in the presence of resorcinol formaldehyde as the carbon precursor and tetraethylenepentamine (TEPA) as nitrogen precursor as well as the base catalyst, followed by carbonization and activation. Their nitrogen content and microstructure of the nitrogen-rich carbon microspheres could be adjusted by varying the addition of TEPA. The significant enhancement of the microstructure and the nitrogen doping leads to high CO<sub>2</sub> adsorption in the activated carbon microspheres. The high nitrogen content of activated sample AMPS-4 was 5.61%, and the large specific surface area and micropore volume were 786.5 m<sup>2</sup>/g and 0.28 cm<sup>3</sup>/g, respectively. The activated sample AMCS-4 had the highest CO<sub>2</sub> adsorption reaching 5.52 mmol/g and 2.97 mmol/g at 0 °C and 25 °C, respectively. Compared with EDA-prepared carbon microspheres AMCS-4E, TEPA-prepared carbon microspheres AMCS-4 have stabler chemical adsorption to CO<sub>2</sub> due to their higher nitrogen content, which is in corresponds to the higher adsorption heat. The introduction of polyvinylpyrrolidone (PVP) into the system as a stabilizer not only improved the monodispersity of carbon microspheres but also improved the adsorption performance of CO<sub>2</sub> by increasing the micropore volume and decreasing the micropore size of the microspheres. The CO<sub>2</sub> adsorption of the PVP-assisted prepared sample AMCS-2-P1 reached 4.48 mmol/g and 2.95 mmol/g at 0 °C and 25 °C respectively, which is 0.72 mmol/g and 0.25 mmol/g higher than that of AMCS-2. The carbon microspheres have high CO<sub>2</sub> dynamic adsorption capacity, excellent selective adsorption, and good cyclic stability.

## Graphical Abstract



✉ Qun-Yan Li  
qyli@bjut.edu.cn

<sup>1</sup> Faculty of Materials and Manufacturing, Beijing University of Technology, 100 Pingleyuan, Chaoyang District, 100124 Beijing, PR China

<sup>2</sup> The Key Laboratory of Advanced Functional Materials, Ministry of Education of China, 100 Pingleyuan, Chaoyang District, 100124 Beijing, PR China

<sup>3</sup> College of Bioscience and Bioengineering, Hebei University of Science and Technology, Shijiazhuang 050018 Hebei Province, PR China

**Keywords** Monodisperse · Nitrogen-rich · Carbon microspheres · CO<sub>2</sub> adsorption

## Highlights

- Monodisperse highly N-rich carbon microspheres were prepared by a one-step hydrothermal method.
- The microspheres have a good monodisperse, improved microstructure, and high N content.
- The microspheres have high CO<sub>2</sub> adsorption capacity, good selective adsorption, and cycling stability.

## 1 Introduction

The climate deterioration observed in recent years, which may be caused by global warming, is a matter of general public concern. CO<sub>2</sub> emissions associated with human activities play an important role in global warming and climate change. Therefore, the reduction of CO<sub>2</sub> emissions is an urgent task and extensive research on viable CO<sub>2</sub> capture technologies is being conducted worldwide. Currently, there are four main types of CO<sub>2</sub> capture technologies: pre-combustion capture technology [1–3], Chemical looping combustion [4, 5], Oxy-fuel combustion carbon capture [6], and post-combustion capture strategies [7]. Post-combustion capture technology is a relatively mature technology suitable for most operating power plants to achieve CO<sub>2</sub> reduction as it does not require major modifications to the original power plant system. The most popular post-combustion capture technologies include membrane separation [8], liquid absorption [9], and solid adsorption [3]. Among the various state-of-the-art CO<sub>2</sub> capture technologies, adsorption by solid adsorbents is considered an effective technique for separating CO<sub>2</sub> from flue gases because of its many advantages, such as simplicity of operation, high efficiency, low energy consumption, and no corrosion problems. Solid adsorbent materials currently used for CO<sub>2</sub> adsorption include zeolites [10–14], mesoporous silica [15–19], metal oxides [20], metal-organic skeletal materials (MOFs) [21–26], carbon-based materials [27], etc. Compared with several other materials, porous carbon-based materials show the advantages of good water/thermal stability, high acid/alkaline resistance, adjustable pore structure, and low cost.

It is generally accepted that the CO<sub>2</sub> adsorption performance of carbon-based materials is mainly influenced by their physisorption and chemisorption. Studies have shown that high microporosity and high nitrogen doping will improve the adsorption performance of carbon materials [28–33]. Different types of nitrogen have different adsorption capacities for CO<sub>2</sub>. Pyridine-type nitrogen in carbon microspheres is more basic than pyrrole-type nitrogen, which is more favorable for chemisorption. Although the experimental reaction process for the preparation of carbon microspheres is complex, the ratio of pyridine-type nitrogen and pyrrole-type nitrogen in the carbon microspheres could be adjusted by changing the nitrogen precursors. In addition, changing the nitrogen precursors affects the nitrogen

content and pore structure of the carbon material. At present, some nitrogen doping precursors such as ammonia [34], ethylenediamine [35, 36], melamine [37, 38] hexamethylenetetramine [39, 40] among which, ethylenediamine are mostly used to synthesize the nitrogen-rich carbon microspheres. Tetraethylenepentamine, an organic amine with both primary and secondary amino groups, has a more complex molecular structure to influence micropore and N-doping than ethylenediamine, its introduction might greatly change the catalytic reaction to influence the microstructure and N-doping of the carbon materials, which have a great effect on the CO<sub>2</sub> adsorption performance. In addition, monodisperse carbon microspheres show better homogeneity and smaller agglomerates, which are more likely to be advantageous in practical industrial applications, with good flowability and separation. In the reported work, PVP was employed as a particle stabilizer and nitrogen source to improve the dispersion and nitrogen content of carbon microspheres [36], but the nitrogen-rich carbon microspheres have rarely been PVP-assisted synthesized especially using TEPA as a nitrogen precursor, and the alkaline catalyst.

In this work, nitrogen-rich carbon microspheres were synthesized using resorcinol and formaldehyde as carbon precursors and TEPA as a nitrogen precursor and the alkaline catalyst by one-pot hydrothermal method. The effect of TEPA on the microstructure and nitrogen doping of the carbon materials was investigated and hence their performance by modulating the doping of TEPA. In addition, the stabilizer PVP was introduced to investigate its effect on prepared carbon microspheres.

## 2 Experiment

### 2.1 Materials

Resorcinol (C<sub>6</sub>H<sub>4</sub>(OH)<sub>2</sub>, 98%), formaldehyde (HCHO, 37 wt%), tetraethylenepentamine, and ethylenediamine were purchased from Fuchen (Tianjin) Chemical Reagent Co., Ltd. and polyvinylpyrrolidone (PVP) was obtained from Shanghai Macklin Biochemical Co., Ltd. Industrial-grade ethanol and deionized water were used for all experiments.

## 2.2 Synthesis of nitrogen-rich carbon materials prepared from TEPA as a nitrogen source

Nitrogen-containing polystyrene microspheres were synthesized using a one-pot hydrothermal method [35, 36]. Namely, an aqueous solution of alcohol was prepared by mixing 24 ml of ethanol and 60 ml of distilled water. Subsequently, different amounts of tetraethylenepentamine (TEPA, the moles of amine to moles of resorcinol were 0.5, 1.5, 2.5, 3.5, 4.5, and 5.5 respectively) were added under continuous stirring. Then, 0.6 g of resorcinol was added and stirred until completely dissolved. Next, 0.84 ml of 37 wt% formaldehyde was slowly added and stirred at 30 °C for 24 h. Finally, the reaction mixture was transferred to a Teflon vessel of 125 mL capacity and placed in a sealed metal autoclave vessel at 100 °C for 24 h. The solid product (nitrogen-containing polymer spheres) was obtained by centrifugation and dried at 100 °C for 12 h. To obtain nitrogen-doped carbon spheres, the prepared nitrogen-doped microspheres were treated with heat treatment in N<sub>2</sub>. The heat treatment in N<sub>2</sub> was carried out in a tube furnace in flowing nitrogen at a heating rate of 1 °C/min to 350 °C for 2 h, followed by a resumption of heating at a rate of 1 °C/min to 600 °C for 4 h. The resulting carbon microspheres are labeled MCS-x; “MCS” denotes carbon spheres and the symbol “x” denotes a designation for the molar ratio of amine to resorcinol. Molar ratios of 0.5, 1.5, 2.5, 3.5, 4.5, 5.5 for amines to resorcinol correspond to MCS-1, 2, 3, 4, 5, 6 respectively. Post-synthesis activation of the carbon spheres was carried out by placing ceramic boats containing 0.2 g MCS in a ceramic tube furnace under flowing nitrogen at a heating rate of 10 °C/min up to 850 °C. After reaching the specified temperature, the activation gas was introduced into the tube furnace (50 cm<sup>3</sup>/min) for 4 h and then switched back to nitrogen to prevent further activation during cooling to room temperature. The activation material obtained is denoted AMCS-x, where “A” indicates activation, in all cases for 4 h at 850 °C CO<sub>2</sub>; the rest of the sample symbol (MCS-x) is the same as in the case of non-activated MCS (see above).

## 2.3 Synthesis of PVP stabilized carbon microspheres

Monodisperse nitrogen polystyrene microspheres were prepared by one-pot hydrothermal method [36]. An aqueous solution of alcohol was prepared by mixing 24 ml of ethanol and 60 ml of distilled water. Subsequently, 0.345 ml of tetraethylenepentamine (TEPA, the ratio of moles of amine group to moles of resorcinol of TEPA was 1.5) was added under continuous stirring. Different amounts of PVP (0.1 g, 0.2 g, 0.3 g) were added to the reaction mixture and stirred for a further 20 min. Then, 0.6 g of resorcinol was added and stirred until completely dissolved. Next, 0.84 ml of

37Wt% formaldehyde was slowly added and stirred at 30 °C for 24 h. The following hydrothermal reaction, carbonization, and activation processes are the same as in 2.2 above. The resulting carbon microspheres are labeled MCS-2-Py; “MCS” indicates carbon spheres, “2” represents the amount of TEPA (the moles of amine to moles of resorcinol was 1.5), the symbol “P” indicates PVP, and the symbol “y” indicates the amount of PVP. For example, the numbers 1, 2, 3 correspond to the addition of 0.1 g, 0.2 g, and 0.3 g of PVP respectively. The activation material obtained is denoted AMCS-2-Py, where “A” indicates activation, and the rest of the sample code symbol (MCS-2-Py) is the same as in the case of non-activated MCS (see above).

## 2.4 Synthesis of nitrogen-rich carbon materials prepared from EDA as a nitrogen source

Nitrogen-containing polystyrene microspheres were synthesized using a one-pot hydrothermal method [35, 36]. Namely, an aqueous solution of alcohol was prepared by mixing 24 ml of ethanol and 60 ml of distilled water. Subsequently, different amounts of tetraethylenepentamine (EDA, the ratio of moles of amine to moles of resorcinol was 1.5, 2.5, and 3.5 respectively) were added under continuous stirring. Then, 0.6 g of resorcinol was added and stirred until completely dissolved. Next, 0.84 ml of 37 wt% formaldehyde was slowly added and stirred at 30 °C for 24 h. The following hydrothermal reaction, carbonization, and activation processes are the same as in 2.2 above. The resulting carbon microspheres are labeled MCS-Ez; “E” represents the EDA, “MCS” denotes carbon spheres and the symbol “z” denotes a designation for the molar ratio of amine to resorcinol. Molar ratios of 1.5, 2.5, 3.5 for amines to resorcinol correspond to MCS-E2, E3, and E4 respectively. The activation material obtained is denoted AMCS-Ez, where “A” indicates activation, and the rest of the sample code symbol (AMCS-Ez) is the same as in the case of nonactivated MCS (see above).

## 3 Characterization

### 3.1 Characterization of porous carbon spheres

Morphology was observed by transmission electron microscopy (TEM, JEM-2010, operating voltage 200 kV) and a Gemini SEM 300 scanning electron microscope. Laser Raman spectroscopy was carried out in a Raman spectrometer (JY-HR800532nm), and the crystal morphology of the microspheres was determined by Cu-K $\alpha$  radiation ( $\lambda = 1.5418 \text{ \AA}$ ) in the range 20° to 80° using a Bruker D8 Advance X-Ray Diffractometer (XRD). The specific surface area, pore size distribution, and pore structure of the

material were determined on a Micromeritics ASAP 2020 specific surface area auto physical adsorber. The test temperature was  $-196\text{ }^{\circ}\text{C}$ . All samples were degassed at  $200\text{ }^{\circ}\text{C}$  for 2 h before adsorption measurements. The BET equation was used to calculate the specific surface area of the samples, and the Horvath-Kawazoe method was used to calculate the pore size distribution and average pore size of the samples. XPS (X-ray photoelectron spectroscopy) measurements were carried out on the ESCALAB 250Xi using a monochromatic Al X-ray source (97.9 W, 93.9 eV).

### 3.2 Adsorption measurements

**Static adsorption:**  $\text{CO}_2$  adsorption measurements were carried out on carbon microspheres at 0 and  $25\text{ }^{\circ}\text{C}$  using an ASAP 2020 volumetric analyzer. All samples were pre-treated at  $200\text{ }^{\circ}\text{C}$  for at least 2 h before sorption measurements. The test pressure range was from 0 to 1 atm.

**Dynamic adsorption:** Dynamic adsorption experiments were carried out in a fixed bed adsorber with a 4 mm inner diameter glass adsorption column and the temperature of the column was controlled by a heating plate. For adsorption, the sample was loaded into the adsorption column and first purged with pure nitrogen gas at a flow rate of 50 ml/min for more than 2 h at  $200\text{ }^{\circ}\text{C}$ , then lowered to room temperature and switched to adsorption gas, and then heating plate temperature was set to  $0\text{ }^{\circ}\text{C}$  for adsorption. During the adsorption process, 0.1 g of adsorbent is filled in a quartz glass tube and a dry carbon dioxide nitrogen gas mixture is passed through the tube at a flow rate of 10 ml/min, the gas flow rate is controlled by an electronic flow meter. The concentrations of all components were determined using a Pfeiffer OmniStar GSD 320 mass spectrometer (MS). The adsorption capacity of the sorbent was calculated from the penetration curve, using the  $\text{CO}_2$  concentration in the inlet gas, the flow rate, the saturation time, and the mass of the sorbent.

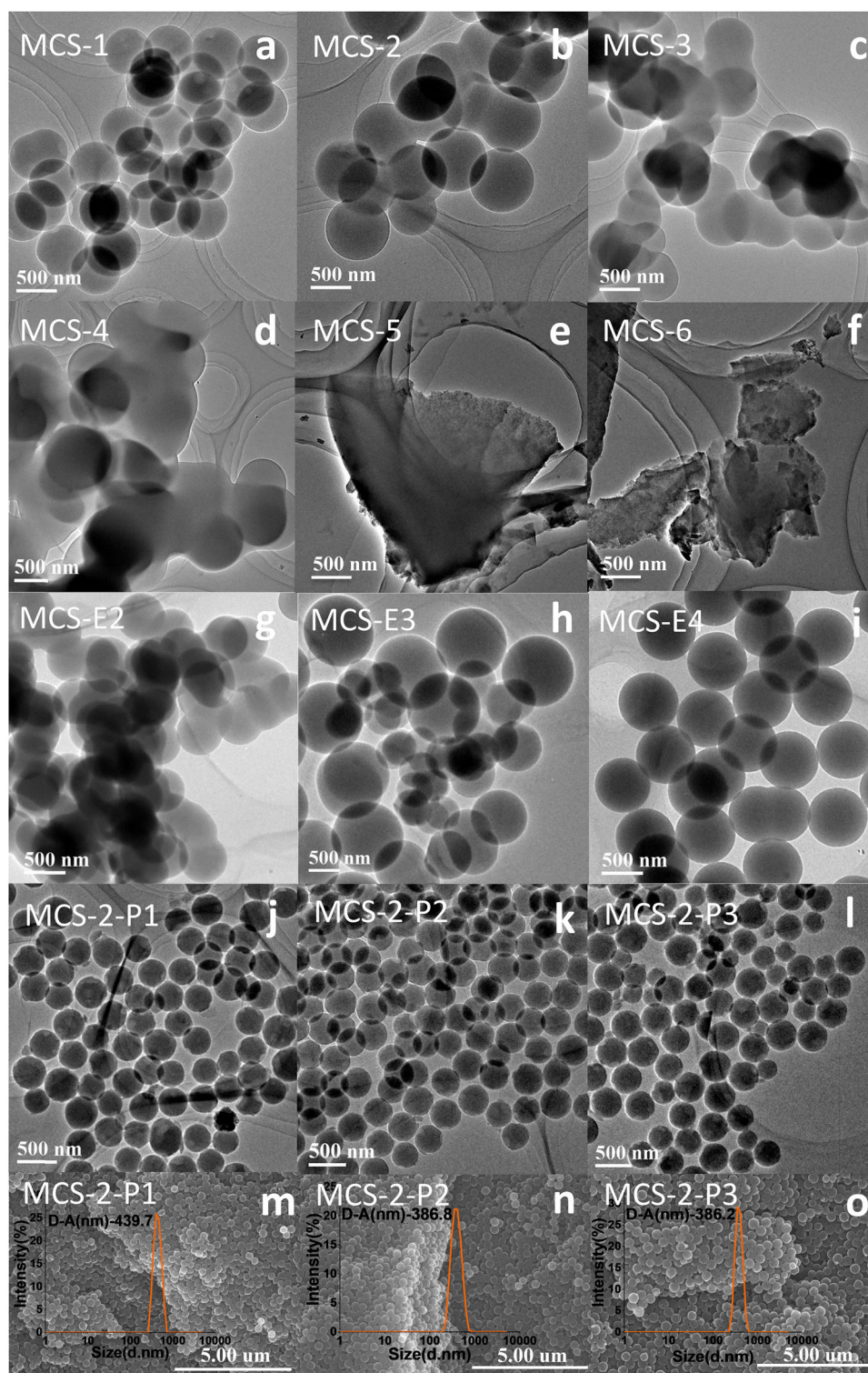
## 4 Results and discussion

TEM and SEM images of the prepared carbon microspheres are shown in Fig. 1. For samples MCS-1, and 2, the microspheres are homogeneous and their average size is about 622.2 nm and 763.8 nm respectively. As the doping of TEPA increases, the dispersion of the sample shows a tendency to decrease, showing some agglomeration. While overviewing MCS-1, 2, 3, and 4, the size homogeneity of the microspheres decreases with increasing TEPA doping and the size is not homogeneous. When the doping of TEPA reaches a certain value, that is, the ratio of the molar number of the amine group to the molar number of resorcinol is 4.5, the carbon material could no longer maintain

the shape of the microsphere and appears irregular bulk, such as MCS-5 and MCS-6. Figure 1 shows that at lower amine molar doping, the TEPA-prepared samples are more likely to be spherical, higher amine molar doping results in more inhomogeneous samples, and when a lot of amines is added, the reaction rate is very fast and prone to agglomeration and non-sphericity. In contrast, the EDA-prepared samples were more homogeneous in sphericity only when doped with higher amine moles. In addition, corresponding to the observation during the reaction process, more and faster turbidity appeared in the TEPA-involved reactive solution than in the EDA-involved reactive solution when the same amine molar doping was added during the reaction. As shown in Fig. 1, the dispersion of carbon microspheres prepared by adding PVP stabilizer is greatly improved, because PVP has carbonyl and nitrogen atoms with a pair of lone electrons, so it can form hydrogen bonds with the hydroxyl group of the polymer sphere. The spatial obstruction of the long vinyl polymer chain prevents the aggregation of the synthesized nanoparticles, resulting in a more uniform size of the final microspheres. As shown in Fig. 1, with the increase of PVP addition, the average size of carbon microspheres decreased, and the average size of MCS-2-P1 and MCS-2-P2 were 439.7 nm and 386.8 nm, respectively. However, when a certain amount of PVP was added, excessive PVP could not be evenly dispersed in the system, and the phenomenon of MCS-2-P3 particles would appear uneven, with many small microspheres. The average size of MCS-2-P3 samples was 386.2 nm. Figure 2 shows SEM images and EDS spectra of samples of AMCS-4, AMCS-E4, and AMCS-2-P1. It can be seen that the distribution of elemental N on the surface of the samples is homogeneous and the nitrogen content of the samples AMCS-4, AMCS-E4, and AMCS-2-P1 is 3.94, 3.04, and 2.02% respectively, indicating that nitrogen-rich carbon microspheres have been successfully prepared.

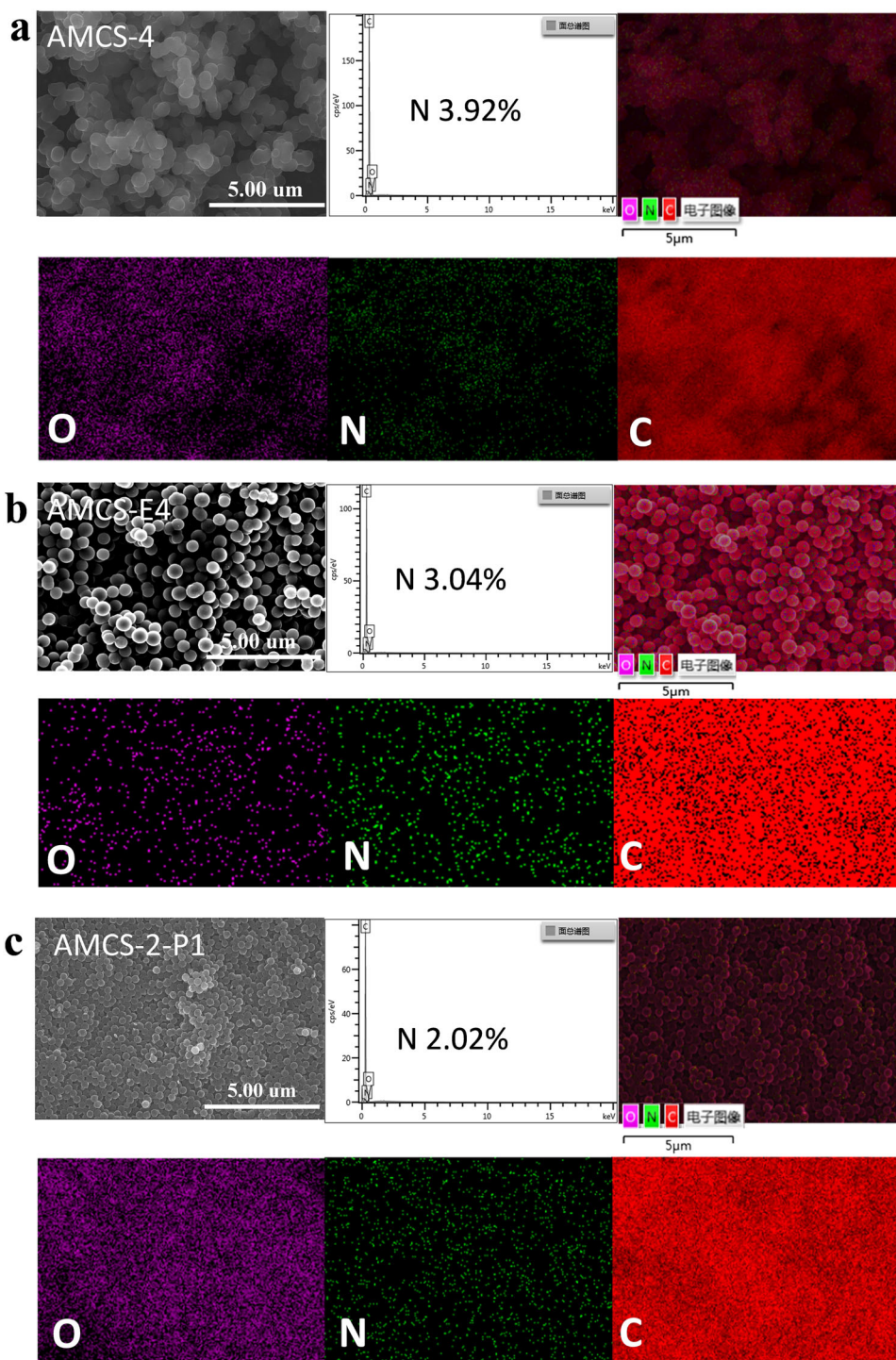
The percentage of nitrogen atoms was assessed by X-ray photoelectron spectroscopy (XPS) analysis. The nitrogen species type and surface elemental composition data obtained by XPS analysis are shown in Table 1 and Fig S1. The nitrogen content in the MCS tends to increase and then decrease with the amount of TEPA in the reaction mixture. In other words, when the molar ratio of the amine group to resorcinol is 0.5-5.5, the percentage of nitrogen atoms in the obtained MCS increases from 3.42%(MCS-1) to 7.19% (MCS-4) and then decreases to about 4.01%(MCS-5). In general, the nitrogen content will be reduced after activation, which could be attributed to the thermal decomposition loss of nitrogen during activation. As can be seen from Table 1, the nitrogen content of TEPA-prepared samples MCS-4 and AMCS-4 is higher than that of EDA-prepared samples MCS-E4 and AMCS-E4. The carbon material prepared with TEPA as a precursor retains more nitrogen

**Fig. 1** TEM, SEM images of prepared carbon microspheres. **a–e** are the TEPA-prepared samples, **g–i** are the TEPA-prepared samples, **j–o** are the PVP-assisted samples



doping, which facilitates the chemisorption of  $\text{CO}_2$  by the carbon spheres. The nitrogen content of MCS-2-P1 and MCS-2-P2 samples supplemented with polyvinylpyrrolidone (PVP) is slightly lower than that of MCS-2, while that of MCS-2-P3 is higher than that of

MCS-2. It is because when the amount of PVP reached a certain level, the hydroxyl group on the surface of the polymer microsphere combined a large amount of PVP in the form of a hydrogen bond, which is retained in the form of pyrrole nitrogen after carbonization. The nitrogen content

**Fig. 2** EDS of (a) AMCS-4, (b) AMCS-E4, and (c) AMCS-2-P1

of the samples prepared by adding PVP decreased after activation due to the decomposition of nitrogen during heat treatment.

Further, High-resolution XPS spectra (N 1s) revealed the morphology of nitrogen in the carbon matrix, as shown in Fig S1. Deconvolution spectra of N 1s with two binding energies of  $398.2 \pm 0.4$  and  $399.9 \pm 0.3$  eV correspond to pyridine nitrogen and pyrrole nitrogen, respectively.

Pyridine nitrogen is more alkaline than pyrrole nitrogen and shows a stronger adsorption capacity for  $\text{CO}_2$ . The anti-fold product XPS spectrum of N 1s in the MCS shows peaks near 401.3 eV and 405.2 eV, which can be attributed to quaternary nitrogen and N-oxide, respectively. High-resolution XPS spectra of (C 1s) and (O 1s) further reveal the morphology of carbon and oxygen in the carbon matrix, as shown in Fig S2. The C spectrum with a binding

**Table 1** Pore structure parameters of a series of prepared carbon microspheres

Sample	$S_{\text{BET}}^{\text{a}}$ (m <sup>2</sup> /g)	$S_{\text{mi}}^{\text{b}}$ (m <sup>2</sup> /g)	$V_{\text{mi}}^{\text{c}}$ (cm <sup>3</sup> /g)	$V_{\text{t}}^{\text{d}}$ (cm <sup>3</sup> /g)	$V_{\text{mi}}/V_{\text{t}}$ (%)	Diameter <sup>e</sup> (nm)	$N^{\text{f}}$ (%)	nCO <sub>2</sub> mmol/g(0 °C)	nCO <sub>2</sub> mmol/g(25 °C)
MCS-1	542.0	479.8	0.19	0.21	90.5	0.59	3.42	2.88	/
MCS-2	537.4	464	0.18	0.20	90.0	0.56	5.34	3.46	2.30
MCS-3	547.4	456.5	0.18	0.23	78.3	0.63	6.53	2.97	/
MCS-4	405.0	323.9	0.13	0.17	76.5	0.63	7.19	2.99	2.49
MCS-5	3.5	/	/	/	/	/	4.52	2.64	/
MCS-6	8.1	/	/	/	/	/	4.94	2.54	/
MCS-E4	468.5	401.5	0.19	0.24	79.2	0.45	5.36	3.14	/
MCS-2-P1	440.1	438.9	0.17	0.18	94.4	0.48	4.28	2.73	/
MCS-2-P2	432.6	386.6	0.18	0.27	66.7	0.46	4.95	2.71	/
MCS-2-P3	444.6	391.3	0.16	0.40	40.0	0.48	6.06	2.70	/
AMCS-1	556.4	490.6	0.20	0.21	95.2	0.62	3.27	3.38	/
AMCS-2	596.2	547.9	0.21	0.24	87.5	0.72	3.92	3.76	2.70
AMCS-3	730.7	677.3	0.26	0.29	89.7	0.62	6.36	4.40	/
AMCS-4	786.5	731.8	0.28	0.32	87.5	0.62	5.61	5.52	2.97
AMCS-5	315.6	295.4	0.11	0.12	91.7	0.63	3.31	4.31	/
AMCS-6	11.4	/	/	/	/	/	2.58	3.93	/
AMCS-E4	628.3	591.0	0.23	0.26	88.5	0.52	4.20	5.60	2.84
AMCS-2-P1	817.5	752.0	0.28	0.38	73.7	0.65	2.38	4.48	2.95
AMCS-2-P2	659.0	615.3	0.23	0.31	74.2	0.63	3.75	3.88	/
AMCS-2-P3	486.7	435.3	0.17	0.25	68.0	0.63	5.36	3.61	/

<sup>a</sup>The BET surface area<sup>b</sup>The microporous BET surface area<sup>c</sup>The microporous volume<sup>d</sup>The total volume<sup>e</sup>The pore size distribution was calculated using the HK method<sup>f</sup>N% is nitrogen weight percentages in carbon spheres

energy of 284.8 eV corresponds to C. The binding energy of 284.8 eV in the C spectrum is associated with C, C = C, and phenyl, 286 eV with C-O, and 289 eV with C = O. The binding energy of 532 eV in the O spectrum is associated with (C-O) and 533 eV with phenol (C-O-H). Notably, MCS samples have a higher binding energy signal of pyridine nitrogen than that of pyrrole nitrogen, indicating there is a higher concentration of the former in them. However, after heat treatment activation, AMCS samples have a higher binding energy signal of pyrrole nitrogen. Fig S1 shows that the ratio of pyridine nitrogen to pyrrole nitrogen in TEPA-prepared samples is similar to that in EDA-prepared samples. In addition, the O1s XPS spectra of MCS-2 and MCS-2-P1 are shown in Fig S2. It can be seen that the C = O peak of MCS-2-P1 is slightly higher than that of MCS-2. This may be due to the introduction of some pyrrolidone (PVP) through the introduction of pyrrolidone, which increases the C = O ratio in the polymer skeleton. Due to the introduction of pyrrole nitrogen in PVP, the proportion of pyridine nitrogen in PVP-assisted prepared carbon microspheres is reduced, which may reduce the chemical adsorption of CO<sub>2</sub> by carbon microspheres.

The nitrogen adsorption and desorption curves of the activated carbon spheres and the corresponding pore diameter increment distribution curves are shown in Fig. 3. All parameters, specific surface area, and pore structure parameters are shown in Table 1. As shown in Table 1, after activation of all carbon spheres, the specific surface area and pore volume will increase. Figure 3a shows activated samples prepared by adding TEPA or EDA. The adsorption isotherms are all type I, indicating that the samples are microporous carbon spheres. As shown in Table 1, the specific surface area of activated carbon spheres prepared by adding TEPA is between 550 and 800 m<sup>2</sup>/g. It can be seen that activated MCS have a high specific surface area, which is mainly due to a large number of fine pores (pore size <1 nm). For example, the micropore volume of AMCS-4 samples was 0.28 cm<sup>3</sup>/g, respectively, which can be read in Table 1. The specific surface area and pore volume of the TEPA-prepared sample AMCS-4 are higher than that of the EDA-prepared sample AMCS-E4. This may be because TEPA is more alkaline and contains more nitrogen atoms in the molecule, which is more likely to participate in the reaction and enter the carbon sphere skeleton, resulting in

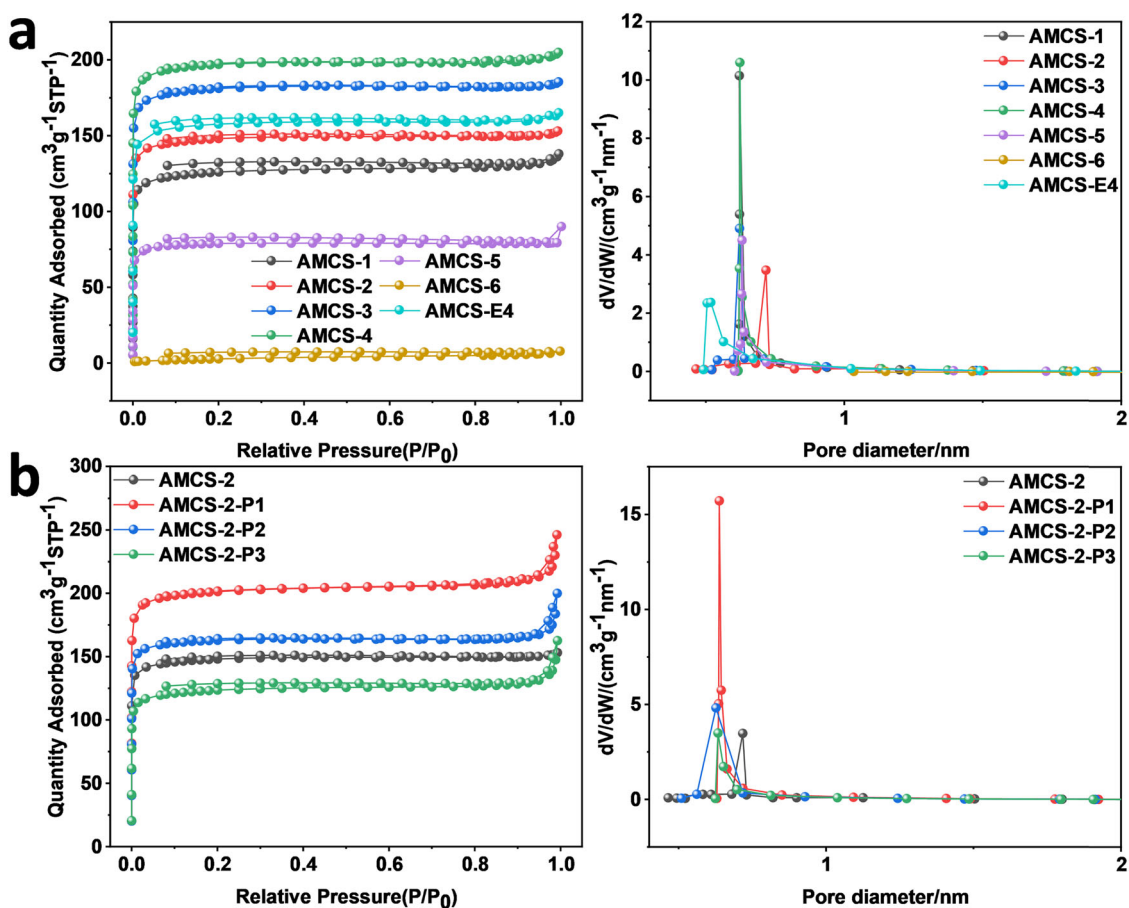


**Fig. 3**  $N_2$  adsorption–desorption isotherms and pore size distributions of a series of activated carbon microspheres. **a** The nitrogen adsorption–desorption isotherm and pore size distribution of activated carbon spheres obtained by changing the amount of TEPA and EDA. **b** The nitrogen adsorption–desorption isotherm and pore size distribution of monodisperse activated carbon spheres obtained by adding PVP

more micropores in the subsequent carbonization process. In this respect, the physical adsorption of samples with TEPA was stronger. As can be seen from Fig. 3a, the maximum pore size of the TEPA-prepared sample AMCS-4 is larger than that of the EDA-prepared sample AMCS-E4, which may be since TEPA molecules are larger than EDA molecules, resulting in micropores with larger pore sizes. In this respect, the physical adsorption of the sample with EDA is stronger.

As can be seen in Table 1 and Fig. S3b, the specific surface area of the non-activated carbon microspheres, MCS-2-P1, MCS-2-P2, and MCS-2-P3, is all lower than that of MCS-2. The specific surface area of activated carbon microspheres AMCS-2-P1 and AMCS-2-P2 is significantly higher than that of AMCS-2, possibly because the introduction of pyrrole nitrogen at this time is easier to decompose into gas to produce more pores in the activation process, resulting in the specific surface area increases. In addition, according to Fig. 3b, it can be seen that the maximum pore size of the PVP-assisted prepared carbon microspheres is smaller than that of the sample

prepared without PVP, which leads to the enhanced physical adsorption of these PVP-assisted prepared carbon microspheres after activation. However, when PVP content reaches a certain level, such as AMCS-2-P3, its specific surface area is significantly lower than that of AMCS-2, which may be due to excessive PVP blocking a large number of micropores in the polymerization process.

Fig S4 shows the XRD pattern of the carbon microspheres. The carbon microspheres with different nitrogen demonstrate similar diffraction peaks corresponding to the (002) graphite peak and the (100) graphite and (101) graphite peaks, implying that the prepared microspheres have been carbonized at 600 °C. The (002) peak is significantly shifted to the left with a reference to the graphite phase standard spectrum, indicating that the activation treatment resulted in a lower degree of graphitization and that the carbon microspheres obtained consisted mainly of microcrystalline graphite filled with defects. This defective structure is often accompanied by the formation of a porous structure, which favors  $CO_2$  adsorption.



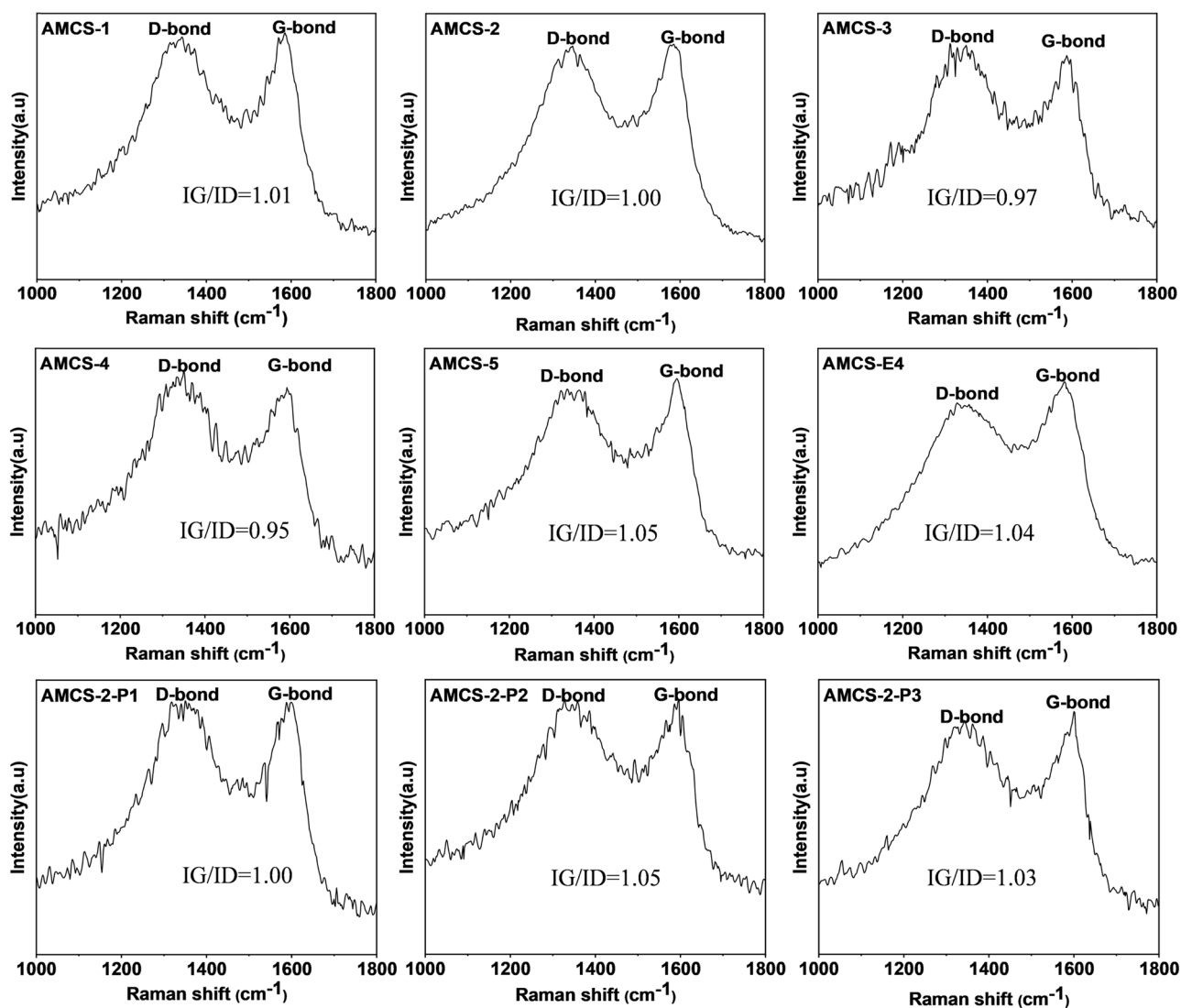
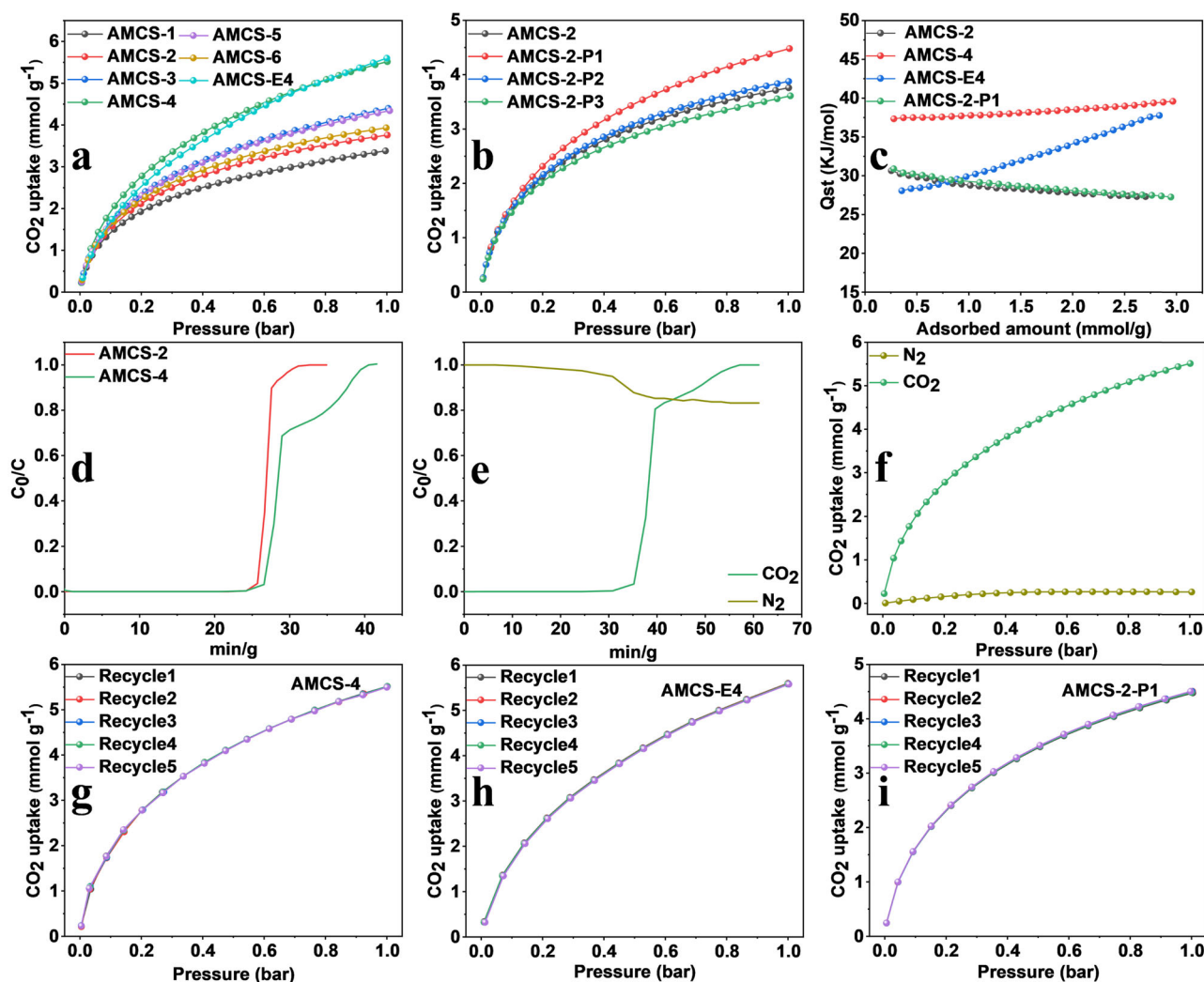


Fig. 4 Raman spectra of activated carbon microspheres

Figure 4 shows the Raman spectra of activated carbon microspheres, which have two peak bands centered on  $1354\text{ cm}^{-1}$  (D band) and  $1583\text{ cm}^{-1}$  (G band). Band D is caused by the disordered and incomplete carbon microcrystals and the tensile vibration of the G band is corresponding to the graphite matrix. The IG/ID value is an important parameter to measure the degree of graphitization of a sample, the lower the value the lower the degree of graphitization. The high relative strengths IG/ID of the samples of AMCS-1 ~ AMCS-5, AMCS-E4, and AMCS-2-P1 ~ AMCS-2-P3 were 1.01, 1.00, 0.97, 0.95, 1.05, 1.04, 1.00, 1.05 and 1.03, respectively. Combined with the Raman spectra of nonactivated carbon microspheres in Fig S6, the IG/ID of MCS-1-MCS-5, MCS-E4, and MCS-2-P1 ~ MCS-2-P3 were 1.20, 1.19, 1.13, 1.13, 1.16, 1.07, 1.23, 1.18 and 1.19, respectively. The range of variation in the reduction of graphitization due to micropores is small,

but can be corroborated by small data changes in IG/ID values, which vary regularly with the pore structure parameters. The activation treatment has lowered the IG/ID value of all samples due to the defects and the generation of micropores in the activation process. With TEPA doping decreasing, the IG/ID values of carbon microspheres decreased first and then increased. The IG/ID value of AMCS-4 was the lowest at 0.95, indicating the poorest graphitization and the most defects in the carbon microspheres, which complained with the largest micropore volume corresponding to that of AMCS-4 in Table 1. Besides, it was found that the IG/ID values of TEPA-prepared samples AMCS-4 and MCS-4 were lower than that of EDA-prepared samples MCS-E4 and AMCS-E4. It indicates that TEPA is more likely to generate more defects and micropores than using EDA, which is in corresponds with the larger micropore volume of the TEPA-prepared



**Fig. 5** CO<sub>2</sub> adsorption isotherms (a, b), heat of adsorption curves (c), dynamic adsorption curves (d), selective adsorption curves (e, f), and cyclic stability curves (g, h and i) of the samples measured under ambient conditions

samples in Table 1. The IG/ID values of the samples of AMCS-2-P1 and AMCS-2-P2 were the same or slightly higher than that of AMCS-2, which may be due to fewer defects caused by the smaller pores of the PVP-assisted prepared samples as shown in Table 1.

The adsorption capacity of carbon microspheres for CO<sub>2</sub> at 0 °C atmospheric pressure (1 bar) was studied. The measured CO<sub>2</sub> adsorption isotherms, adsorption heat curves, selective adsorption curves, and cyclic stability curves of samples under environmental conditions are shown in Fig. 5. Compared with Fig S6, it is found that the adsorption performance of activated samples is all promoted compared with those nonactivated samples since the activation treatment increased the specific surface area and pore volume of the samples, which is the key to improving the adsorption performance. As can be seen in Fig. 5a, the CO<sub>2</sub> adsorption capacity of the sample at 0 °C firstly increased

and then decreased with the increase of TEPA addition, among which the CO<sub>2</sub> adsorption capacity of sample AMCS-4 is the highest, reaching 5.52 mmol/g at 0 °C. AMCS-4 has the highest CO<sub>2</sub> adsorption capacity, which is consistent with its high specific surface area, pore volume, and nitrogen content. The adsorption of AMCS-4 and AMCS-E4 at 1 bar and 0 °C are compared. And it can be seen from Fig. 5a that the adsorption capacity of carbon spheres prepared by TEPA and EDA is similar. Combined with the analysis in Table 1, the TEPA-prepared samples have a high nitrogen doping, specific surface area, and microporous volume, which is beneficial for their chemisorption and physical adsorption of carbon dioxide. However, the TEPA-prepared samples show larger micropores, which may not be conducive to the physical adsorption of carbon dioxide. Therefore, the adsorption capacity of the TEPA-prepared samples is comparable to that of the EDA-

prepared samples. However, from the point of view of the heat of adsorption, as shown in Fig. 5c, the TEPA-prepared samples have a higher adsorption heat, indicating that the TEPA-prepared samples have a higher chemical adsorption capacity for CO<sub>2</sub> due to their higher nitrogen content.

Due to the introduction of alkaline adsorption sites by nitrogen doping in the sample, the binding force of the sample on CO<sub>2</sub> molecules increases with the increase of organic amine content, and the adsorption heat curve generally conforms to this adsorption law, as shown in Fig. 5c, AMCS-2, and AMCS-4. However, the actual adsorption performance is still affected by the synergistic effect of pore structure and alkaline adsorption sites. Combined with Table 1, it can be seen that the specific surface area and micropore volume of the sample AMCS-4 are the largest, the nitrogen content is lower than that of AMCS-3, but the CO<sub>2</sub> adsorption capacity is the highest, indicating that the pore structure of the sample AMCS-4 has the best synergistic effect of pore structure and the alkaline active site. As shown in Fig. 5c, this is demonstrated by the large adsorption heat of sample AMCS-4 in the range of 37–40 kJ/mol, because the large adsorption heat indicates that it has strong thermodynamic adsorption. In general, during the adsorption process for some carbon microspheres such as AMCS-2, the most active sites such as basic nitrogen functional groups and ultrapores are first occupied, and then adsorbed to other weaker binding sites, usually leading to a gradual decline in Q<sub>st</sub>. However, as to the other samples with high micropore volume such as AMCS-4, the Q<sub>st</sub> value increases with the increase of CO<sub>2</sub> absorption. It is because when the carbon microspheres with high micropore volume have large CO<sub>2</sub> adsorption, the enhancement of gas and gas interactions in samples may lead to the increase of adsorption heat since the adsorption heat is influenced by the combination of gas and surface, gas and gas interactions [41].

The adsorption performance curves of PVP-assisted prepared samples AMCS-2-P1 ~ AMCS-2-P3 compared with AMCS-2 are shown in Fig. 5b. The CO<sub>2</sub> adsorption performance of AMCS 2-P1 and AMCS 2-P2 is better than that of AMCS-2. The CO<sub>2</sub> adsorption capacity of AMCS-2-P1 was 4.48 mmol/g at 1 bar and 0°C, which was 0.72 mmol/g higher than that of AMCS-2. The results in Table 1 and Fig. 6, demonstrate that AMCS-2-P1 has a larger CO<sub>2</sub> adsorption capacity compared with AMCS-2, which reason might be its higher specific surface area and higher micropore volume compensating for the influence of its lower nitrogen content on its CO<sub>2</sub> adsorption performance. However, excessive PVP will clog the micropores of the prepared carbon microspheres, such as MCS-2-P3, which also has a lower specific surface area after activation, resulting in a lower CO<sub>2</sub> adsorption capacity. what's more, the reduced maximum pore size of the PVP-

assisted synthesized samples is also conducive to CO<sub>2</sub> adsorption.

In addition, a dynamic CO<sub>2</sub> adsorption study was carried out under a simulated dynamic environment. The penetration curves are shown in Fig. 5d. Based on the penetration curves, CO<sub>2</sub> concentration, flow rate, saturation time, and adsorbent mass were used to calculate the CO<sub>2</sub> adsorption capacity of the adsorbent. The CO<sub>2</sub> adsorption capacity of AMCS-2 and AMCS-4 were 3.62 mmol/g and 4.10 mmol/g, respectively. The CO<sub>2</sub> dynamic adsorption capacity was lower than the theoretical value of static adsorption but still had a high adsorption capacity. Figure 5e, f shows the selective adsorption curves of CO<sub>2</sub>/N<sub>2</sub> under dynamic and static conditions respectively. It can be seen that under the same conditions, carbon microspheres absorb more CO<sub>2</sub> and almost no N<sub>2</sub>, and this selective adsorption is conducive to industrial applications. Figure 5g, h, i respectively show the cyclic adsorption curves of samples AMCS-4, AMCS-E4, and AMCS-2-P1. It can be seen that the samples have good cyclic stability, and the adsorption capacity is almost unchanged after five cycles.

A comparative schematic of several different carbon spheres is shown in Fig. 6. As shown, under alkaline conditions, formaldehyde forms a nitrogen-containing polymer backbone with TEPA and resorcinol to form a polymer backbone with pyrrole and pyridine-type nitrogen. On the one hand, TEPA is an alkaline catalyst, facilitating the reaction to produce carbon spheres. On the other hand, TEPA is involved in the reaction as a nitrogen-doped precursor. In addition, it can be seen from the previous discussion that the TEPA-prepared samples had more micropores and higher nitrogen content after activation compared to the EDA-prepared samples. This favorable CO<sub>2</sub> chemisorption can be attributed to the fact that the TEPA-prepared samples retained more nitrogen before activation, decomposed more nitrogen during activation, and retained more nitrogen after activation. In addition, the samples prepared with TEPA also had more micropores that were favorable for physisorption, but on the other hand, the maximum pore size of the sample AMCS-4 prepared by TEPA was 0.62 nm and the maximum pore size of the sample AMCS-E4 prepared by EDA was 0.52 nm. The larger pore size of the sample AMCS-4 prepared by TEPA was not conducive to physical adsorption, probably because the TEPA molecule was larger than the EDA molecule.

The possible reaction mechanism for the introduction of PVP into the system for the synthesis of carbon microspheres is also shown in Fig. 6, where the introduced PVP is hydrogen-bonded to the polymer backbone. The carbon microspheres prepared are well monodispersed due to the spatial resistance of the PVP macromolecules. At the same time, PVP contains pyrrole-type nitrogen, which is also involved in the reaction into the carbon material backbone,

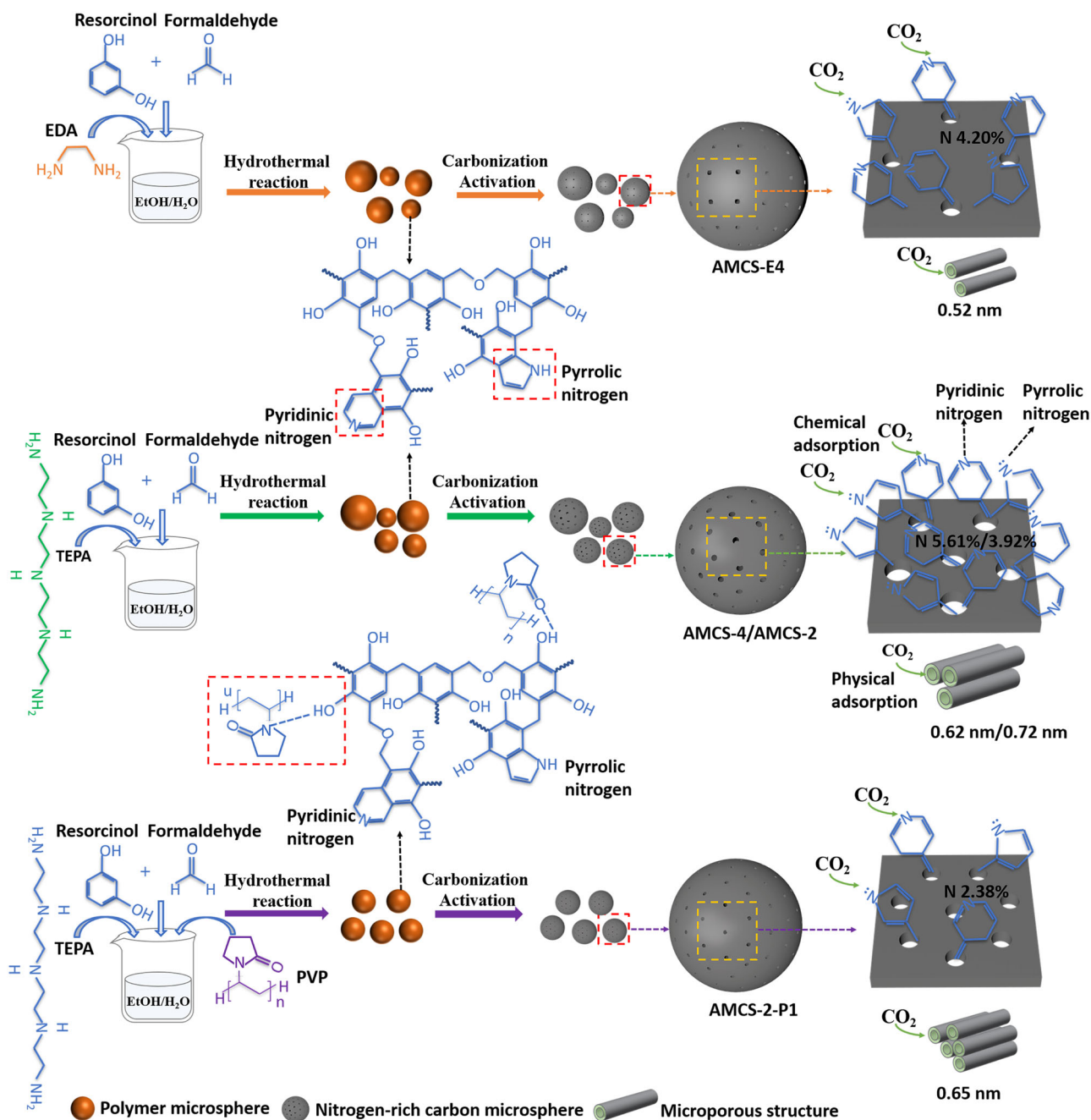


**Fig. 6** Possible mechanisms for the synthesis of different nitrogen-rich carbons

leading to a change in nitrogen doping. After introducing a certain amount of PVP, the proportion of pyrrole-type nitrogen in the carbon microspheres decreases. Since pyridine-type nitrogen is a stronger chemisorbed of  $\text{CO}_2$  than pyrrole-type nitrogen, it may reduce the chemisorption of carbon spheres. Pyrrole-type nitrogen decomposes more readily at high temperatures, resulting in lower nitrogen content in the activated carbon spheres, which increases the specific surface area and micropore volume of the carbon spheres. In addition, the most available pore sizes of the PVP-assisted samples were smaller

than those prepared without the addition of PVP, for example, the maximum pore sizes of AMCS-2-P1 for AMCS-2 were 0.65 nm and 0.72 nm respectively, which facilitated the physical adsorption of  $\text{CO}_2$  by the activated carbon microspheres.

In general, high specific surface area, high micropore volume, high nitrogen content, and small micropore pore size are beneficial for  $\text{CO}_2$  adsorption by carbon microspheres. The  $\text{CO}_2$  adsorption capacity of activated carbon microspheres in Table 1 is plotted against the different influencing factors as shown in Fig. 7. It was found that the

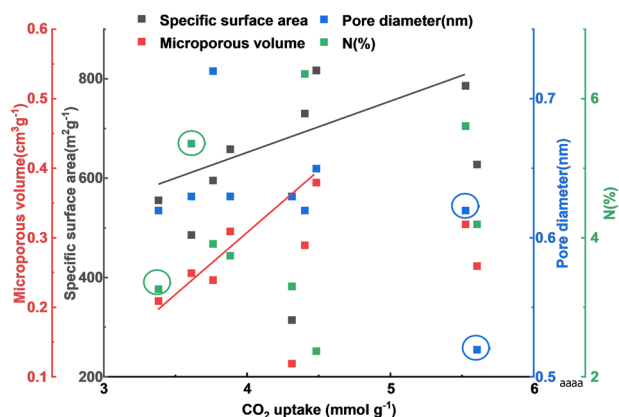


**Fig. 7** Diagram of the CO<sub>2</sub> adsorption capacity of carbon microspheres in relation to different influencing factors

CO<sub>2</sub> adsorption capacity of carbon microspheres was mainly related to specific surface area and micropore volume in a positive correlation.

## 5 Conclusions

The main factors affecting the CO<sub>2</sub> adsorption performance of carbon microspheres are the specific surface area, pore volume, pore size, and nitrogen content of the microsphere. The activation treatment can increase the specific surface area and pore volume of the samples. The specific surface area and pore volume of the TEPA-prepared sample AMCS-4 obtained were 786.5 m<sup>2</sup>/g and 0.28 cm<sup>3</sup>/g, respectively, and the nitrogen content was 5.61%. In this case, AMCS-4 has the highest CO<sub>2</sub> adsorption capacity due to the synergistic effect between the micropore volume and the nitrogen content and the adsorption of CO<sub>2</sub> at 0 °C and 25 °C reached 5.52 mmol/g and 2.97 mmol/g, respectively. AMCS-4 had good selective adsorption performance and cycle stability. Compared with EDA, the TEPA-prepared samples can obtain spherical particles under smaller nitrogen doping. It shows higher nitrogen doping and larger micropore volume, which is conducive to carbon dioxide adsorption. However, it has larger micropores, which may not be conducive to the physical adsorption of CO<sub>2</sub>, but can be used as a basic template for later surface modification to further improve the carbon adsorption performance. At present, the adsorption capacity of the TEPA-prepared sample is similar to the EDA-prepared sample, but the adsorption heat of the TEPA-prepared sample is higher and has stronger adsorption stability. The PVP-assisted prepared carbon microspheres not only have good dispersion but also have improved CO<sub>2</sub> adsorption performance due to their higher specific surface area, larger micropore volume, and smaller micropore. The specific surface area, micropore volume, and maximum micropore size of AMCS-2-P1 were

817.5 m<sup>2</sup>/g, 0.28 cm<sup>3</sup>/g, and 0.65 nm, respectively. Under the conditions of 1 bar, 0 °C, and 25 °C, the CO<sub>2</sub> adsorption capacity of AMCS 2-P1 was 4.48 mmol/g and 2.95 mmol/g, respectively, which were 0.72 mmol/g and 0.25 mmol/g higher than that of AMCS-2 prepared without PVP. The carbon microspheres have high CO<sub>2</sub> dynamic adsorption capacity, excellent selective adsorption, and good cyclic stability.

**Acknowledgements** We would like to thank the support of National Natural Science Fund for Innovative Research Groups (Grant No. 51621003).

## Compliance with ethical standards

**Conflict of interest** The authors declare no competing interests.

**Supplementary information** The online version contains supplementary material available at <https://doi.org/10.1007/s10971-023-06165-z>.

## References

- Sánchez-Laínez J, Zornoza B, Téllez C (2018) Asymmetric polybenzimidazole membranes with thin selective skin layer containing ZIF-8 for H<sub>2</sub>/CO<sub>2</sub> separation at pre-combustion capture conditions. *J Membr Sci* 563:427–434. <https://doi.org/10.1016/j.memsci.2018.06.009>
- Wu F, Dellenback PA, Fan M (2019) Highly efficient and stable calcium looping based pre-combustion CO<sub>2</sub> capture for high-purity H<sub>2</sub> production. *Materials Today Energy* 13(C). <https://doi.org/10.1016/j.mtener.2019.05.013>
- Gizer SG, Polat O, Ram MK (2022) Recent developments in CO<sub>2</sub> capture, utilization, related materials, and challenges. *Int J Energy Res* 46(12):16241–16263. <https://doi.org/10.1002/er.8347>
- Alalwan HA, Alminshid AH (2021) CO<sub>2</sub> capturing methods: Chemical looping combustion (CLC) as a promising technique. *Sci Total Environ* 788:147850. <https://doi.org/10.1016/j.scitotenv.2021.147850>
- Czakiert T, Krzywanski J, Zylka A (2022) Chemical looping combustion: a brief overview. *Energies* 15(4):1563. <https://doi.org/10.3390/en15041563>
- Yadav S, Mondal SS (2022) A review on the progress and prospects of oxy-fuel carbon capture and sequestration (CCS) technology. *Fuel* 308:122057. <https://doi.org/10.1016/j.fuel.2021.122057>
- Akeeb O, Wang L, Xie W (2022) Post-combustion CO<sub>2</sub> capture via a variety of temperature ranges and material adsorption process: A review. *J Environ Manag* 313:115026. <https://doi.org/10.1016/j.jenvman.2022.115026>
- Norahim N, Yaisanga P, Faungnawakij K (2018) Recent membrane developments for CO<sub>2</sub> separation and capture. *Chem Eng Technol* 41(2):211–223. <https://doi.org/10.1002/ceat.201700406>
- Ochedi FO, Yu J, Yu H (2021) Carbon dioxide capture using liquid absorption methods: a review. *Environ Chem Lett* 19(1):77–109. <https://doi.org/10.1007/s10311-020-01093-8>
- Garshasbi V, Jahangiri M, Anbia M (2017) Equilibrium CO<sub>2</sub> adsorption on zeolite 13X prepared from natural clays. *Appl Surf Sci* 393:225–233. <https://doi.org/10.1016/j.apsusc.2016.09.161>
- Kim M, Lee JW, Kim S (2022) CO<sub>2</sub> adsorption on zeolite 13X modified with hydrophobic octadecyltrimethoxysilane for indoor

- application. *J Clean Prod* 337:130597. <https://doi.org/10.1016/j.jclepro.2022.130597>
12. Kwon D, Kim JC, Lee H (2022) Engineering micropore walls of beta zeolites by post-functionalization for CO<sub>2</sub> adsorption performance screening under humid conditions. *Chem Eng J* 427:131461. <https://doi.org/10.1016/j.cej.2021.131461>
  13. Kareem FAA, Shariff AM, Ullah S (2018) Experimental measurements and modeling of supercritical CO<sub>2</sub> adsorption on 13X and 5A zeolites. *J Nat Gas Sci Eng* 50:115–127. <https://doi.org/10.1016/j.jngse.2017.11.016>
  14. Saisuwasiri P, Worathanakul P (2019) A study of CO<sub>2</sub> thermodynamic adsorption and desorption with bi-metal loading on zeolite Y. *Mater Today: Proc* 17:1458–1465. <https://doi.org/10.1016/j.matpr.2019.06.168>
  15. Watabe T, Yogo K (2013) Isotherms and isosteric heats of adsorption for CO<sub>2</sub> in amine-functionalized mesoporous silicas. *Sep Purif Technol* 120:20–23. <https://doi.org/10.1016/j.seppur.2013.09.011>
  16. Wang X, Li H, Liu H (2011) AS-synthesized mesoporous silica MSU-1 modified with tetraethylenepentamine for CO<sub>2</sub> adsorption. *Microporous Mesoporous Mater* 142(2–3):564–569. <https://doi.org/10.1016/j.micromeso.2010.12.047>
  17. Ma J, Liu Q, Chen D (2014) CO<sub>2</sub> adsorption on amine-modified mesoporous silicas. *J Porous Mater* 21(5):859–867. <https://doi.org/10.1007/s10934-014-9835-2>
  18. Sari Yilmaz M (2021) The CO<sub>2</sub> adsorption performance of aminosilane-modified mesoporous silicas. *J Therm Anal Calorim* 146(5):2241–2251. <https://doi.org/10.1007/s10973-020-10417-3>
  19. Başaran K, Topçubaşı BU, Davran-Candan T (2021) Theoretical investigation of CO<sub>2</sub> adsorption mechanism over amine-functionalized mesoporous silica. *J CO<sub>2</sub> Utilization* 47:101492. <https://doi.org/10.1016/j.jcou.2021.101492>
  20. Mat N, Timmiati SN, Teh LP (2022) Recent development in metal oxide-based core-shell material for CO<sub>2</sub> capture and utilisation. *Applied Nanoscience* 1–21. <https://doi.org/10.1007/s13204-022-02559-7>
  21. Qasem NAA, Ben-Mansour R, Habib MA (2018) An efficient CO<sub>2</sub> adsorptive storage using MOF-5 and MOF-177. *Appl Energy* 210:317–326. <https://doi.org/10.1016/j.apenergy.2017.11.011>
  22. Xu G, Meng Z, Guo X (2019) Molecular simulations on CO<sub>2</sub> adsorption and adsorptive separation in fullerene impregnated MOF-177, MOF-180 and MOF-200. *Comput Mater Sci* 168:58–64. <https://doi.org/10.1016/j.commatsci.2019.05.039>
  23. Jun HJ, Yoo DK, Jhung SH (2022) Metal-organic framework (MOF-808) functionalized with ethyleneamines: Selective adsorbent to capture CO<sub>2</sub> under low pressure. *J CO<sub>2</sub> Utilization* 58:101932. <https://doi.org/10.1016/j.jcou.2022.101932>
  24. Wibowo AH, Hasanah YIF, Firdaus M (2018) Efficient CO<sub>2</sub> adsorption by Cu (II) acetate and itaconate bioproduct based MOF. *J Environ Chem Eng* 6(2):2910–2917. <https://doi.org/10.1016/j.jece.2018.04.031>
  25. Gaikwad S, Kim Y, Gaikwad R (2021) Enhanced CO<sub>2</sub> capture capacity of amine-functionalized MOF-177 metal organic framework. *J Environ Chem Eng* 9(4):105523. <https://doi.org/10.1016/j.jece.2021.105523>
  26. Khan MR, Harp S, Neumann J (2016) Processing and performance of MOF (metal organic framework)-loaded PAN nanofibrous membrane for CO<sub>2</sub> adsorption. *J Mater Eng Perform* 25(4):1276–1283. <https://doi.org/10.1007/s11665-016-1966-y>
  27. Abd AA, Othman MR, Kim J (2021) A review on application of activated carbons for carbon dioxide capture: present performance, preparation, and surface modification for further improvement. *Environ Sci Pollut Res* 28(32):43329–43364. <https://doi.org/10.1007/s11356-021-15121-9>
  28. Rehman A, Heo YJ, Nazir G (2021) Solvent-free, one-pot synthesis of nitrogen-tailored alkali-activated microporous carbons with an efficient CO<sub>2</sub> adsorption. *Carbon* 172:71–82. <https://doi.org/10.1016/j.carbon.2020.09.088>
  29. Dassanayake AC, Jaroniec M (2018) Activated polypyrrole-derived carbon spheres for superior CO<sub>2</sub> uptake at ambient conditions. *Colloids Surf A: Physicochem Eng Asp* 549:147–154. <https://doi.org/10.1016/j.colsurfa.2018.04.002>
  30. Wang X, Zhou J, Xing W (2017) Resorcinol-formaldehyde resin-based porous carbon spheres with high CO<sub>2</sub> capture capacities. *J Energy Chem* 26(5):1007–1013. <https://doi.org/10.1016/j.jechem.2017.07.010>
  31. Kim HS, Kim M, Kang MS (2018) Bioinspired synthesis of melaninlike nanoparticles for highly N-doped carbons utilized as enhanced CO<sub>2</sub> adsorbents and efficient oxygen reduction catalysts. *ACS Sustain Chem Eng* 6(2):2324–2333. <https://doi.org/10.1021/acssuschemeng.7b03680>
  32. Choma J, Stachurska K, Marszewski M (2016) Equilibrium isotherms and isosteric heat for CO<sub>2</sub> adsorption on nanoporous carbons from polymers *Adsorption* 22(4):581–588. <https://doi.org/10.1007/s10450-015-9734-0>
  33. Shi J, Cui H, Xu J (2022) N-doped monodisperse carbon nanospheres with high surface area for highly efficient CO<sub>2</sub> capture. *Sep Purif Technol* 290:120822. <https://doi.org/10.1016/j.seppur.2022.120822>
  34. Wickramaratne NP, Jaroniec M (2013) Activated carbon spheres for CO<sub>2</sub> adsorption. *ACS Appl Mater Interfaces* 5(5):1849–1855. <https://doi.org/10.1021/am400112m>
  35. Wickramaratne NP, Xu J, Wang M (2014) Nitrogen enriched porous carbon spheres: attractive materials for supercapacitor electrodes and CO<sub>2</sub> adsorption. *Chem Mater* 26(9):2820–2828. <https://doi.org/10.1021/cm5001895>
  36. Ghimire PP, Dassanayake AC, Wickramaratne NP (2019) Polyvinyl pyrrolidone-assisted synthesis of size-tunable polymer spheres at elevated temperature and their conversion to nitrogen-containing carbon spheres. *J Colloid Interface Sci* 549:162–170. <https://doi.org/10.1016/j.jcis.2019.04.059>
  37. Wang Z, Sun L, Xu F (2016) Synthesis of N-doped hierarchical carbon spheres for CO<sub>2</sub> capture and supercapacitors. *RSC Adv* 6(2):1422–1427. <https://doi.org/10.1039/C5RA20484D>
  38. Wickramaratne NP, Jaroniec M (2014) Tailoring microporosity and nitrogen content in carbons for achieving high uptake of CO<sub>2</sub> at ambient conditions. *Adsorption* 20(2):287–293. <https://doi.org/10.1007/s10450-013-9572-x>
  39. Liu L, Xie ZH, Deng QF (2017) One-pot carbonization enrichment of nitrogen in microporous carbon spheres for efficient CO<sub>2</sub> capture. *J Mater Chem A* 5(1):418–425. <https://doi.org/10.1039/C6TA09782K>
  40. Liu L, Deng QF, Hou XX (2012) User-friendly synthesis of nitrogen-containing polymer and microporous carbon spheres for efficient CO<sub>2</sub> capture. *J Mater Chem* 22(31):15540–15548. <https://doi.org/10.1039/C2JM31441J>
  41. Xu J, Cui H, Shi J (2018) Agar-derived nitrogen-doped porous carbon for CO<sub>2</sub> adsorption. *ChemistrySelect* 3(39):10977–10982. <https://doi.org/10.1002/slct.201802031>

**Publisher's note** Springer Nature remains neutral with regard to jurisdictional claims in published maps and institutional affiliations.

Springer Nature or its licensor (e.g. a society or other partner) holds exclusive rights to this article under a publishing agreement with the author(s) or other rightsholder(s); author self-archiving of the accepted manuscript version of this article is solely governed by the terms of such publishing agreement and applicable law.